Non-Invasive Characterization of Atrial Flutter Mechanisms Using Recurrence Quantification Analysis on the ECG: A Computational Study

Giorgio Luongo , *Member, IEEE*, Steffen Schuler, *Member, IEEE*, Armin Luik,
Tiago P. Almeida , *Member, IEEE*, Diogo C. Soriano , Olaf Dössel , *Senior Member, IEEE*,
and Axel Loewe , *Member, IEEE*

Abstract—*Objective:* Atrial flutter (AFl) is a common arrhythmia that can be categorized according to different self-sustained electrophysiological mechanisms. The non-invasive discrimination of such mechanisms would greatly benefit ablative methods for AFl therapy as the driving mechanisms would be described prior to the invasive procedure, helping to guide ablation. In the present work, we sought to implement recurrence quantification analysis (RQA) on 12-lead ECG signals from a computational framework to discriminate different electrophysiological mechanisms sustaining AFl. *Methods:* 20 different AFl mechanisms were generated in 8 atrial models and were propagated into 8 torso models via forward solution, resulting in 1,256 sets of 12-lead ECG signals. Principal component analysis was applied on the 12-lead ECGs, and six RQA-based features were extracted from the most significant principal component scores in two different approaches: individual component RQA and spatial reduced RQA. *Results:* In both approaches, RQA-based features were significantly sensitive to the dynamic structures underlying different AFl mechanisms. Hit rate as high as 67.7% was achieved when discriminating the 20 AFl mechanisms. RQA-based features estimated for a clinical sample suggested high agreement with the results found in the computational framework. *Conclusion:* RQA has been shown an effective method to distinguish different AFl electrophysiological mechanisms in a non-invasive computational framework. A clinical 12-lead ECG used as proof of concept showed the value of both the simulations and the methods. *Significance:* The non-invasive discrimination of AFl mechanisms helps to delineate the ablation strategy, reducing time and resources required to conduct invasive cardiac mapping and ablation procedures.

Index Terms—Atrial flutter, 12-lead ECG, non-invasive, biosignal processing, spatio-temporal, recurrence, RQA, nonlinear dynamic, PCA, cardiac modeling.

I. INTRODUCTION

ATRIAL flutter (AFl) is a common reentrant arrhythmia with 200,000 new annual cases estimated for the U.S. population [1]. This arrhythmia is characterized by self-sustained mechanisms and electrical signals that regularly propagate along various physiological pathways [2]–[4]. Although AFl is not a direct cause of death, it can cause significant symptoms and complications - e.g., palpitations, dyspnea, stroke and heart attacks.

Among the cardiac arrhythmias, the mechanisms perpetuating AFl have been extensively investigated and are relatively well known. This includes right atrial (RA) tachycardia [5]–[7] and left atrial (LA) AFl forms [8]–[10], occurrences after ablation for atrial fibrillation (AFib) [11]–[13] and macro reentrant mechanisms [14]. However, the characterization of the dynamical structures underlying electrophysiological (EP) phenomena from the perspective of non-linear and non-invasive time series analysis is still lacking. In fact, AFl mechanisms are usually discriminated from invasive intracardiac signals [3], [15], whereas non-invasive methods - using traditional 12-leads ECGs, for instance - are mostly used for the clinical detection of AFl with respect to AFib [16]. The non-invasive discrimination of AFl mechanisms would help to delineate the ablation strategy, reducing time and resources required to conduct invasive cardiac mapping and ablation procedures. Different AFl mechanisms

might culminate in different dynamic structures that could be captured by non-invasive data. The nature of this problem suggest that recurrence quantification analysis (RQA) might offer an interesting solution for the investigation of the underlying cardiac dynamic.

Interestingly, the development of RQA itself is intrinsically related to the analysis of cardiac signals. For instance, the work by Trulla *et al.* highlighted the promising applications of RQA on biomedical signals [17], describing the advantages of using RQA on investigating nonstationary and short-time cardiac datasets [18], [19]. Since then, RQA has been extensively used for characterizing the dynamics of heart rate variability [20], [21], cardiac restitution [22], or even combined with machine learning techniques for sudden cardiac death stratification [23] and ECG-based arrhythmia classification [24], [25], among other applications. RQA has been used to specifically characterize the dynamics of intracardiac signals during cardiac disorders [26], [27], [28], [29]. These investigations have shown that RQA-based features represent a promising set of tools to identify phase transitions and discriminate different EP characteristics related to the atrial tissue. Finally, Yang has proposed using recurrence plots (RPs) and RQA to analyze the spatial vectocardiogram for identifying cardiac disorders, being able to detect myocardial infarction with an average sensitivity of 96.5% and an average specificity of 75% [30].

In the present work, we sought to characterize different AFl mechanisms from the perspective of multivariate surface potentials and nonlinear time series. The present methodology stands out from previous investigations for considering an *in silico* ground truth followed by a clinical case application. The study was divided in two arms considering simulated 12-lead ECG signals: individual component RQA (icRQA) and (a novel) spatial reduced RQA (srRQA). The results suggest that RQA is effective in characterizing and discriminating the dynamic structures from distinct AFl mechanisms, and might help to define novel protocols for clinical planning and ablation strategy.

II. METHODS

A. Simulated AFl Scenarios

A database with computational AFl scenarios was organized based on: AFl mechanisms commonly described in the literature [31], [32]; documented clinical AFl cases [5]–[13]; and computational studies conducted in a previous work by Oesterlein *et al.* [33].

Cardiac excitation was modelled using the fast marching approach to solve the Eikonal equation [34], [35]. Propagation was simulated on the triangulated volumetric meshes of 8 biatrial anatomies, generated from segmented magnetic resonance imaging (MRI) data of healthy male and female subjects [36]. Interatrial connections were generated by a rule-based algorithm [37], [38]. Scars were added circumferentially around ipsilateral pulmonary veins (PVs), representing ablation scars from previous PV isolations.

In total, 20 mechanisms/scenarios of AFl were implemented, including right atrial (RA) flutter as well as left atrial (LA) forms like macroreentry around the valves (sc1-4), across the roof

TABLE I
DATABASE OF MANUALLY PARAMETERIZED AFL MECHANISMS

Mechanism	Atrium	Position	Direction	ID
Macroreentry	RA	Tricuspid Valve	ccw	sc1
Macroreentry	RA	Tricuspid Valve	cw	sc2
Macroreentry	LA	Mitral Valve	ccw	sc3
Macroreentry	LA	Mitral Valve	cw	sc4
Scar-related Reentry	LA	LPV	post	sc5
Scar-related Reentry	LA	LPV	ant	sc6
Scar-related Reentry	LA	RPV	post	sc7
Scar-related Reentry	LA	RPV	ant	sc8
Figure-8 Macroreentry	LA	Both PVs	ant	sc9
Figure-8 Macroreentry	LA	Both PVs	post	sc10
Figure-8 Macroreentry	LA	RPVs	ant	sc11
Focal Source	LA	RSPV anterior		sc12
Focal Source	LA	RSPV posterior		sc13
Focal Source	LA	LSPV anterior		sc14
Focal Source	LA	LSPV posterior		sc15
Microreentry	LA	ant MV annulus		sc16
Microreentry	LA	ant LAA		sc17
Microreentry	LA	ant RSPV		sc18
Figure-8 Microreentry	LA	ant		sc19
Microreentry	LA	post wall		sc20

Right atrium (RA), left atrium (LA), left pulmonary vein (LPV), right pulmonary vein (RPV), pulmonary veins (PVs), right superior pulmonary vein (RSPV), left superior pulmonary vein (LSPV), mitral valve (MV), left atrial appendage (LAA), clockwise (cw), counterclockwise (ccw), anterior (ant), posterior (post), scenario (sc).

(sc9-11), focal ectopy (sc12–15), and microreentries mediated by scars (sc5-8) or slow conduction areas (sc16-20). A complete list of scenarios is provided in Table I. For scar-related microreentry mechanisms, revitalized atrial tissue was introduced representing the critical isthmus. The 20 different AFl scenarios were constructed by changing the conduction velocity (CV) and refractory period, introducing heterogeneities in the atrial tissue. The simulations were initiated by manually placed triggers and refractory areas. They were continued for at least 5 s to confirm a stable excitation pattern.

The simulated excitation resulted in local activation times (LAT) for each anatomical node that was not isolated. The LATs were extracted in an interval of the simulation in which the specific AFl was formed. These LATs were projected on a new geometry (identical to the previous one), containing only the surface endo-\epicardial layers [37] in order to obtain a vector of LATs only from the surfaces. The transmembrane voltage (TMV) was calculated from the LATs using the Courtemanche *et al.* mathematical remodelled model of the human atrial action potential [39]. The TMV was used to estimate the body surface potential map (BSPM) onto 8 different triangulated surface models of torsos (9,951 nodes and 19,898 triangles on average). The torsos were generated by segmented MRI data of healthy male and female subjects [36], [40]. The boundary element method (BEM) was used to solve the forward problem of electrophysiology [41]. Finally, traditional bipolar ECGs were extracted from the BSPM, including the 12-lead ECGs [42].

Every 12-lead ECG signal has a length of 5 AFl loops and sampling frequency of 1 kHz. Since the ventricles were not included in the simulations, the resulting ECG signals contain only atrial activity represented by the P-waves (also called flutter waves or F-waves), without the QRS complex and T-wave (representing ventricular activity), since the ventricles are not included in the simulations (Fig. 1A-C).
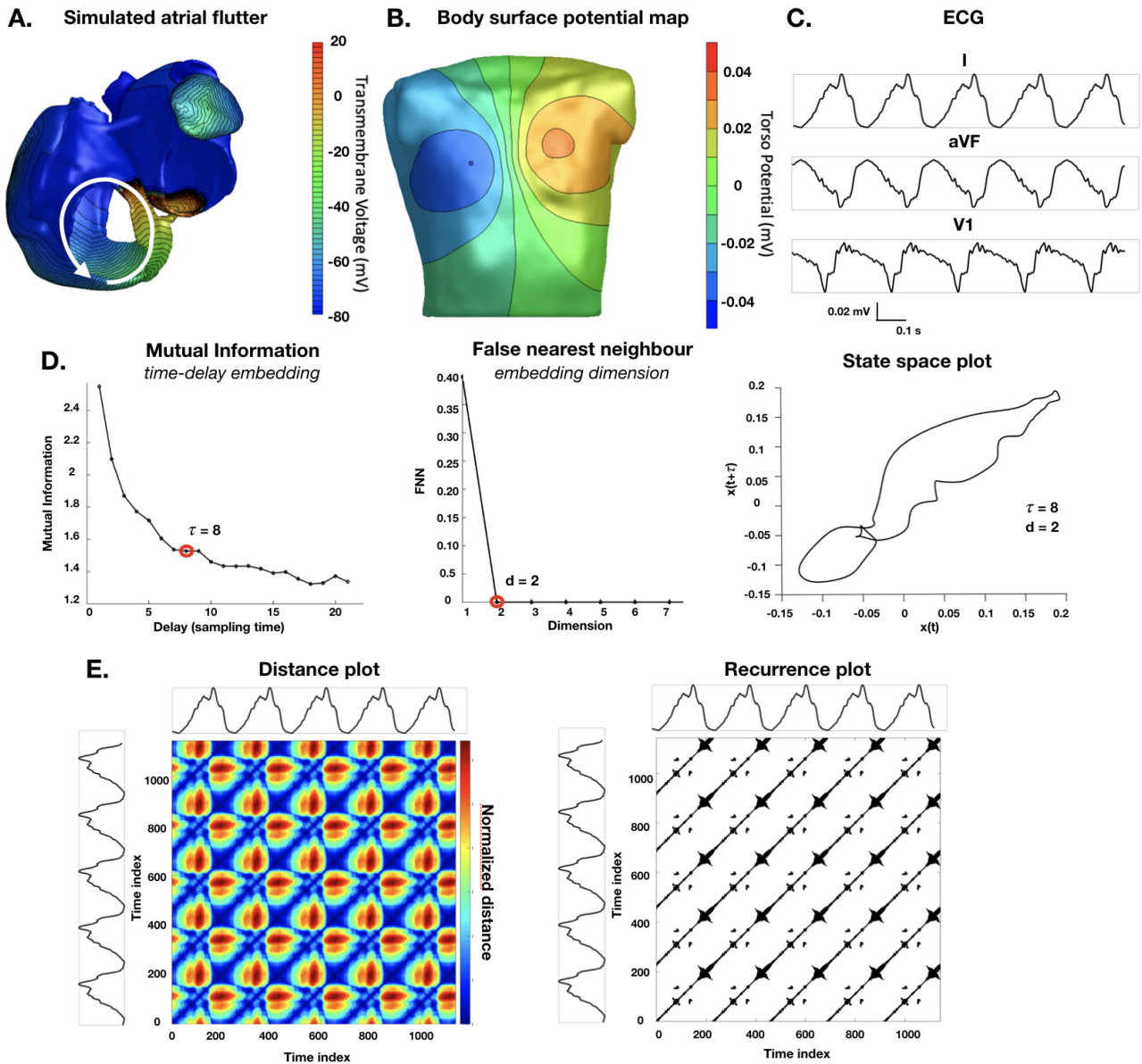
Fig. 1. (A). Illustration of a simulated atrial flutter around the tricuspid valve with ccw direction on one of the atrial models generated from MRI. (B). Example of a BSPM on one of the torso models generated from MRI. The torso potential has been obtained solving the forward problem of electrophysiology from the simulated TMV on the atria. (C). Example of three of the 12-lead ECG signals extracted from the BSPM. Five complete loops of the AFl were taken into consideration. Principal component analysis (PCA) has been applied on the 12-lead ECGs. (D). Illustration of the state space reconstruction following Takens' theorem, with the corresponding time-delay embedding (τ) and embedding dimension (d). (E). The resulting distance plot based on the state space map and the subsequent recurrence plot (RP) after applying an adaptive threshold ε on the distance plot.

A total of 1,256 sets of 12-lead ECG were calculated from the 20 AFl simulated scenarios on 8 atria models and 8 torso models. Due to the proximity of the left inferior pulmonary vein to the mitral valve on one of the atrial models, the left pulmonary vein isolation blocked the signal propagation between these two anatomical points, hindering the implementation of scenarios sc12, sc13, and sc30 on this atria geometry.

B. Non-Redundant Spatial Information of ECGs

The 12-lead ECG signals were organized in a $N \times M$ matrix - where M is the number of leads and N is the number of samples on the leads - and principal component analysis (PCA) was applied. PCA is a linear transformation of a set of variables $\mathbf{X} = (X_1, X_2,.., X_n)^{\mathrm{T}}$ [43]. This technique transforms the data with respect to an orthogonal basis Φ, such that the projections of $\mathbf{X}$ in this new coordinate system have maximum variance. The orthogonal vectors φ^{i} conforming Φ are ordered by decreasing variances. The variance of a variable is an important measure of its amount of information. Every component of the orthogonal basis Φ is called principal component (PC) and the projections of $\mathbf{X}$ with respect to that basis are called principal component scores - PCS, first PCS (PCS 1), second PCS (PCS 2), third PCS (PCS 3). PCA is primarily used for reduction of dimensionality of a

dataset while retaining the most relevant information contained in it [44], [45].

In the present work, PCA was used to reduce the size of each simulated 12-leads ECGs to the PCs that represent a cumulative variance greater than 95% of the total variance. This transformation aims to provide a new set of observations that considers the representative information of the electrical atrial dynamics collected from different sensors (i.e., non-redundant spatial diversity) [42]. PCA also allows to reduce the RQA computational cost, since we can proceed with a reduced space, as explained in II-D.

C. Embedding Parameters and RQA Features

A RP is a two-dimensional graphical technique introduced by Eckmann *et al.* [46], aiming to analyse the structure of multidimensional dynamical system's attractors [21]. It captures the reappearance of multidimensional states by means of a binary matrix $R_{i,j}$, associating the value 1 - represented by a black pixel - whenever states $\mathbf{x}_i$ and $\mathbf{x}_j$ are close to each other by ε, and 0 otherwise. The binary pattern exhibited in the RP is related to the underlying generative dynamics of the observation and can be used to assess different oscillatory properties characterized by diagonal lines - which capture the co-evolution of states in the phase space - and vertical lines - which capture the tendency of remaining in a given state [21]. The systematic quantification of the binary patterns in the RP defines the roots of RQA [18], and, currently, engenders a wide set of metrics that characterize the oscillatory behavior and also allow access to nonlinear invariants - e.g., correlation dimension, Kolmogorov entropy [21], [47] - and information theory [21].

When a single observation is available, the state space can be reconstructed using Takens' theorem [21], which aims to reveal a possible hidden low dimensional trajectory underlying the observation and, consequently, laminar RP structures - diagonals, verticals etc - as shown in Fig. 1D, [28]. In this case, auxiliary axes are defined as delayed samples of the uni-dimensional observation $\mathbf{x}(k)$, such as

$$\mathbf{x}(k) = \{x(k), x(k-\tau), \ldots, x[k-(d_e-1)\tau]\}, \quad (1)$$

in which d_e is the embedding dimension - number of coordinates used for the $\mathbf{x}(k)$ representation - and τ represents the time-delay embedding among samples. These parameters are usually estimated by means of the false nearest neighbor test and the first local minimum of the self-mutual information [21], [48]. In this case, the recurrence matrix ($R_{i,j}$) can be defined in terms of the distance between the respective reconstructed states $\mathbf{x}^i$ and $\mathbf{x}_j$ and a chosen distance threshold ε, which can be expressed as:

$$R_{i,j}(\varepsilon) = \theta\{\varepsilon - \|\mathbf{x}_i - \mathbf{x}_j\|\}, \quad (2)$$

being θ the Heaviside function (Fig. 1E).

For a RP obtained from a time series of N samples, with frequency distribution $P(l)$ of diagonal line length, frequency distribution $P(v)$ of vertical line length, probability $p(l)$ of finding a diagonal of length l, and probability $p(v)$ of finding a

vertical line of length v, the RQA is associated with representative statistical measures of the matrix $R_{i,j}$ [21], used in the present work:

- The recurrence rate (RR), which represents the density of points in a RP:

$$RR = \frac{1}{N^2} \sum_{i,j=1}^{N} R_{i,j}. \quad (3)$$

- The ratio between recurrence points that form diagonal structures (with length $l \geq l_{min}$), referred to as determinism (DET):

$$DET = \frac{\sum_{l=l_{min}}^{N} lP(l)}{\sum_{l=1}^{N} lP(l)}. \quad (4)$$

- The Shannon entropy of diagonal lines in a RP (ENTR_diag), which can be considered as a measure of RPs complexity or organization in terms of the distribution of the diagonal lines:

$$ENTR\_diag = - \sum_{l=l_{min}}^{N} p(l) \ln p(l). \quad (5)$$

- The ratio between recurrence points that form vertical structures (with length $v \geq vmin$), referred to as laminarity (LAM):

$$LAM = \frac{\sum_{v=v_{min}}^{N} vP(v)}{\sum_{v=1}^{N} vP(v)}. \quad (6)$$

- The trapping time (TT), which represents the average length of the vertical lines:

$$TT = \frac{\sum_{v=v_{min}}^{N} vP(v)}{\sum_{v=v_{min}}^{N} P(v)}. \quad (7)$$

- The Shannon entropy of vertical lines in a RP (ENTR_vert), which can be considered as a measure of the RPs complexity or organization in terms of the distribution of the vertical lines:

$$ENTR\_vert = - \sum_{v=v_{min}}^{N} p(v) \ln p(v). \quad (8)$$

D. icRQA and srRQA

Two different RQA paradigms based on different premises were implemented to investigate the underlying dynamics and spatio-temporal structures of the AFl mechanisms. Therefore, the hyper-parameters for each paradigm (icRQA and srRQA) are expected to differ. Both paradigms were implemented considering the PCSs extracted from the simulated 12-lead ECGs.

1) icRQA: The first RQA paradigm (individual component RQA, icRQA) reconstructed the attractors following Takens' Theorem - same procedure as described in Section II-C - for each PCS considered relevant on the basis of their variance. In this case, each PCS had its own time delay and dimension embedding.

2) srRQA: The second - and novel - RQA paradigm (spatial reduced RQA, srRQA) defined the "embedding dimension" based on the number of selected PCSs and, therefore, did not consider Takens' Theorem for attractor reconstruction. Indeed, srRQA considers the first PCS1 as the first coordinate of the observed trajectory, PCS 2 as second coordinate, and so forth - i.e., it defines the AFl trajectory in the domain of PCSs. This leads to a space-time "embedding space" based on the uncorrelated PCSs to obtain minimal redundant spatial information. Consequently, no time embedding procedure was needed for the srRQA since the PCSs are already uncorrelated. The number of PCSs used to reconstruct the state space was chosen based on the best compromise between: the RR value; the maximum phase space diameter portion (maximum distance found in the distance plot); and the discrimination between the 20 AFl scenarios as explained in the following [48]. Once the state space was estimated, the procedure for calculating the RP was the same as described in Section II-C.

E. Defining Hyper-Parameters for RQA

After obtaining the respective state vectors for both paradigms, ε was determined. Previous works have suggested that ε should be chosen such that the resulting RR is approximately 1%, or ε should not exceed 10% of the maximum phase space diameter [21], [49]. Therefore, 12 and 10 different values for ε were tested for the icRQA and srRQA, varying from 0.5% to 11%, and from 1% to 10% of the maximum phase space diameter, respectively. Some preliminary results on the icRQA showed no need to test values lower and higher than the 10 selected for srRQA. For each ε, RR was calculated and the discrimination between the 20 different AFl scenarios was evaluated using the MATLAB function rankfeatures ("CriterionValue" set to "roc"). Hence, ε was defined looking for a suitable compromise among the resulting RR (not too high compared to the recommended 1%), the portion of the maximum phase space diameter (not exceeding 10%), and the discrimination between the 20 AFl scenarios.

Similarly, the minimum line lengths for the calculation of DET and LAM were defined considering the discrimination between the 20 different AFl scenarios. Using ε as defined above, both DET and LAM were calculated for 20 values of minimum line length, varying from 2 to 21 for both icRQA and srRQA. The minimum line lengths were also defined as a compromise between the resulting values for DET and LAM and the 20 AFl scenarios discrimination.

A more detailed description of the selection of optimal values for the hyper-parameters can be found in Almeida *et al.* [28].

F. Clinical Data Sample

A sample of clinical 12-lead ECG was used to evaluate the recurrence plots and RQA-based features obtained in the computational framework. The ECGs were collected during an episode of microreentrant AFl in the LA (1 kHz sampling frequency), representing sc17 (ant LAA, Table I). The AFl mechanism was identified and labelled by inspecting the LAT map recorded with a high density 3D electroanatomical mapping system (Rhythmia HDx, Boston Scientific). The signals were notch filtered at 50 Hz, band-pass filtered between 0.05 Hz - 100 Hz. The portion of signals between two QRS-T complexes was manually extracted from the 12-lead ECGs in order to extract the F-wave component related to the AFl activity. More precisely, all P-waves enclosed between the end of a T-wave until the following QRS complex were extracted.

Both icRQA and srRQA paradigms were tested on the clinical sample. The respective RQA-based features were extracted and compared with those obtained *in silico* to verify agreement between the clinical and synthetic scenarios.

All the experimental procedures were in accordance with the ethical standards of the responsible committee on human experimentation (institutional and national) and with the Helsinki Declaration of 1975, as revised in 2000. All patients provided written informed consent.

G. Statistical Analysis

All continuous normally distributed variables are expressed as mean $\pm$ SD. All continuous non-normally distributed variables are expressed as median $\pm$ interquartile range.

Non-parametric data were analyzed using the Kolmogorov-Smirnov test. The comparison between the 20 AFl scenarios was done using the Kruskal-Wallis non-parametric one-way analysis of variance [50], [51].

An iterative binary classification - AFl scenario vs. all other AFl scenarios - was computed to create receiver operating characteristic (ROC) curves. The ROC curves were computed using the MATLAB function perfcurve and the single RQA-based features as discriminators. The optimum sensitivity and specificity on the ROC curve was defined as the point on the curve with the shortest distance to the top left corner of the graph. Validation of the optimum point of operation for the classification was performed with leave-one-out cross-validation (LOOCV). p-values of less than 0.01 were considered statistically significant.

III. RESULTS

A. PCA on the 12-Lead ECGs

Twelve PCs were estimated from the 12-lead ECGs using PCA, and only the main five were considered, explaining $99.97 \pm 0.03\%$ of the total variance. The icRQA paradigm was implemented on the first three PCSs since they explained $99.10 \pm 0.94\%$ of all variance. For the srRQA, however, different numbers of PCSs were tested to define the optimal number of dimensions. Up to five PCs were tested in descending order of total variance explanation, in which a PCS was added as a new dimension at each iteration, starting with the two main dimensions - PCS 1 and 2.

B. icRQA on Different AFl Mechanisms

1) Hyper-Parameters: The ε was tested for PCSs 1, 2, and 3. The area under the ROC curves (AUCROCs) for these PCSs suggest that 5% of the maximum phase diameter represents a suitable compromise among the resulting RR, the portion of the maximum phase space diameter, and the discrimination between
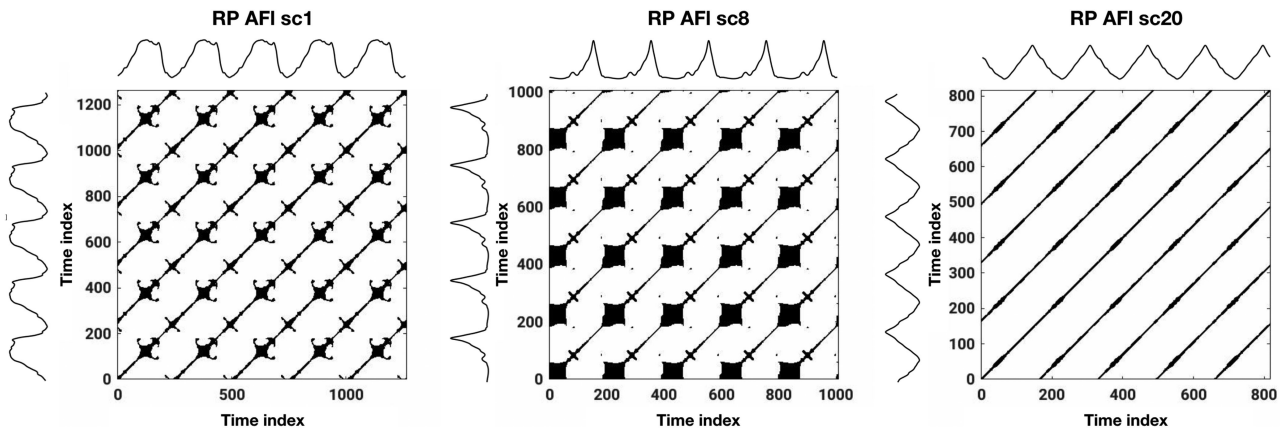
Fig. 2.   The effect of different AFl scenarios in the icRQA-based features. The RPs created for the PCS 1 calculated from the 12-lead ECGs extracted from the same atria and torso combination for three different AFl mechanisms. These examples show how different AFl mechanisms produced different icRQA RPs, highlighting the usefulness of the proposed method for discriminating these different mechanisms.
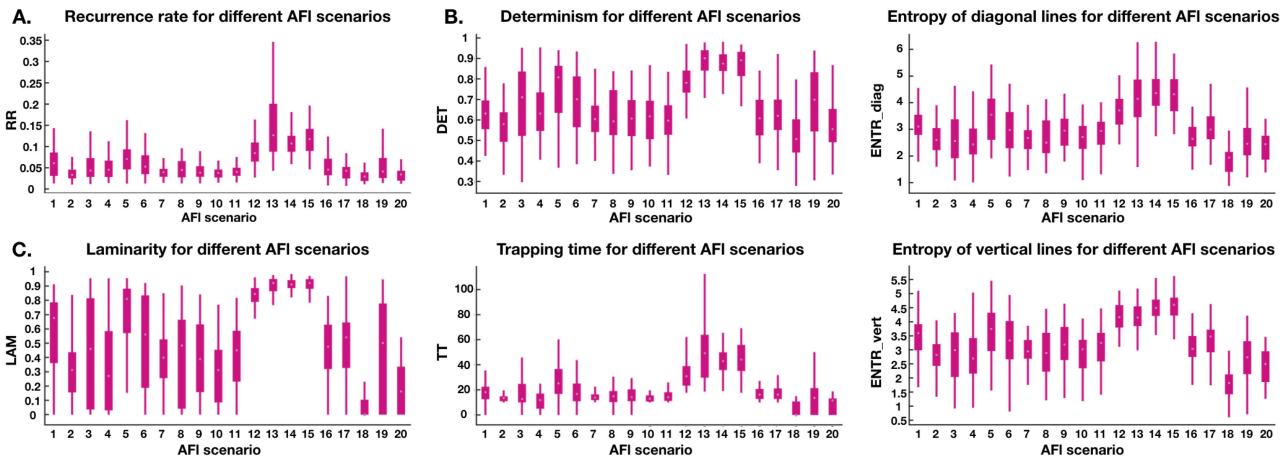
Fig. 3.   Effects of the 20 different AFl scenarios on the icRQA features calculated from PCS 3. (A). RR attribute. (B). Features related to diagonal lines. (C). Features related to vertical lines.

the 20 AFl scenarios. Similarly, the AUCROC values suggest that a minimal diagonal line length of 13, 16, 13 should be considered for the calculation of DET using the PCSs 1, 2, and 3, respectively, and a minimal vertical line length of 10, 11, 8 should be considered for the calculation of LAM. Other values of the maximum phase space diameter and minimal vertical or diagonal line length lead to higher AUCROC and maximal/minimal DET or LAM. However, this may be associated with an undesirable saturation behavior. Further details on these results are provided in the *Supplementary Materials*.

These hyper-parameters were used for the construction of the RPs and the evaluation of icRQA-based features for PCS 1, 2, and 3 in the subsequent parts of the study.

2) Discrimination of AFl Mechanisms: The RPs highlighted visual differences in dynamic structures peculiar to each AFl mechanism (Fig. 2). The icRQA-based features extracted from the PCS 3 between the 20 AFl scenarios are shown in Fig. 3.

All the icRQA features extracted from the individual PCSs (1, 2 and 3) showed significant differences ($p < 0.001$) between the AFl mechanisms. The RPs from all AFl scenarios and the comparisons of the icRQA features within individual PCSs 1 and 2 are shown in the *Supplementary Materials*.

Sc18 resulted in the lowest values for all 6 icRQA features extracted from the three PCSs, whereas sc12, 13, 14, and 15 showed highest median values. Sc12, 13, 14, and 15 were always significantly different from all other cases for all icRQA features across the 3 PCSs. As exceptions, it can be noticed that: 1) PCS 1 DET and RR have shown no significant differences between sc12 vs. all other AFl scenarios; 2) PCS 2 ENTR_diag and PCS 1 TT for sc13 did not differ from all other AFl scenarios; 3) Sc5 has shown no significant differences from sc12, 13, 14, and 15 for any icRQA-based features for PCS 1.

Finally, the icRQA features were effective in discriminating the 20 AFl scenarios, with LOOCV hit rate as high as 67.7% (Table II).

C. srRQA on Different AFl Mechanisms

1) Hyper-Parameters: A similar protocol was followed for defining ε to the srRQA paradigm, the number of dimensions,

TABLE II

ROC CURVES FOR THE DISCRIMINATION OF 20 AFL SCENARIOS USING THE ICRQA-BASED FEATURES (MEAN±SD)

PCS 1	RR	DET	LAM	TT	ENTR_diag	ENTR_vert
AUCROC	0.618±0.002	0.636±0.002	0.681±0.002	0.645±0.002	0.640±0.002	0.674±0.002
Sensitivity	0.323±0.002	0.341±0.002	0.294±0.002	0.378±0.003	0.363±0.003	0.346±0.002
Specificity	0.569±0.002	0.602±0.003	0656±0.003	0.687±0.003	0.636±0.001	0.701±0.002
LOOCV hit rate	0.616±0.045	0.627±0.058	**0.677±0.069**	0.642±0.069	0.632±0.058	0.674±0.082
PCS 2	RR	DET	LAM	TT	ENTR_diag	ENTR_vert
AUCROC	0.625±0.002	0.629±0.0.002	0.669±0.0.002	0.652±0.0.002	0.630±0.0.002	0.663±0.0.002
Sensitivity	0.419±0.003	0.385±0.003	0.325±0.002	0.387±0.002	0.358±0.002	0.297±0.003
Specificity	0.670±0.001	0.643±0.001	0.668±0.002	0.691±0.002	0.626±0.002	0.625±0.002
LOOCV hit rate	0.621±0.059	0.627±0.076	0.627±0.088	0.644±0.096	0.629±0.072	0.659±0.087
PCS 3	RR	DET	LAM	TT	ENTR_diag	ENTR_vert
AUCROC	0.655±0.002	0.654±0.0.002	0.673±0.0.002	0.668±0.0.002	0.655±0.0.002	0.667±0.0.002
Sensitivity	0.263±0.002	0.224±0.002	0.222±0.001	0.246±0.003	0.254±0.0.002	0.281±0.002
Specificity	0.573±0.002	0.538±0.001	0.609±0.003	0.604±0.001	0.566±0.001	0.617±0.002
LOOCV hit rate	0.653±0.091	0.649±0.083	0.649±0.095	0.665±0.100	0.651±0.081	0.665±0.102
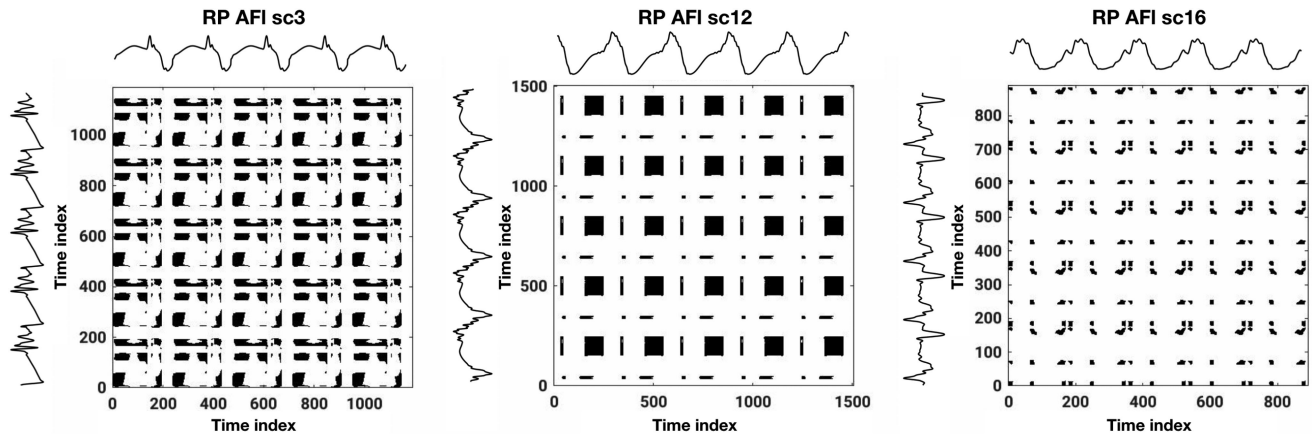
Fig. 4. The effect of different AFl scenarios in the srRQA. The RPs created using two different PCS as dimensions for three different AFl mechanisms. These examples showed how different AFl mechanisms produced different srRQA RPs, making the method promising in characterizing these several mechanisms.

and the minimal vertical/diagonal line length. The AUCROC values suggest that 5% of the maximum phase diameter and 3 as the number of dimensions with a good compromise among the resulting RR, the portion of the maximum phase space diameter, the discrimination between the 20 AFl scenarios and the computational complexity. Similarly, the AUCROC values suggest that a minimum diagonal line length of 6 should be considered for the calculation of DET, and a minimum vertical line length of 7 for the calculation of LAM to obtain a high class discrimination and also minimal and maximal bounds to the attributed estimates. Note that other values of the maximum phase space diameter and minimal vertical or diagonal length lead to higher AUCROC and maximal DET or LAM. These, however, may be associated to an undesirable saturation behavior. Further details on these results are provided in the *Supplementary Materials*.

The obtained srRQA hyper-parameters were used for the construction of the RPs and the evaluation of the RQA-based features in the subsequent parts of this work.

2) Discrimination of AFls: The RPs estimated following the srRQA paradigm also helped to highlight the differences in the dynamic structures peculiar to each AFl scenario (Fig. 4).

Comparisons of the srRQA-based features within the 20 AFl scenarios are shown in Fig. 5.

All the srRQA features exhibited significant differences (p < 0.001) between the AFl mechanisms. The RPs for all AFl scenarios are shown in the *Supplementary Materials*.

Sc12, 14, and 15 exhibited highest values for all the srRQA features, whereas sc18 showed lowest values for all the features except for RR, where sc20 had the lowest distribution values. Sc12, 14, and 15 were significantly different from all other cases and features. Sc5 and sc13 have shown no significant differences from sc12, 14, and 15 for any srRQA features.

Finally, the srRQA-based features were effective in discriminating the 20 AFl scenarios with LOOCV hit rate as high as 65.4% (Table III).

D. AFl Characterization Using RQA-Based Features

Diagonal lines - related to deterministic structures - were found in all RPs calculated with the icRQA, Fig. 2, whereas deteriorated diagonal lines were found with the srRQA - blocks of recurrence, Fig. 4. Opposite situation for vertical lines - related to laminar structures that were found principally with the srRQA,
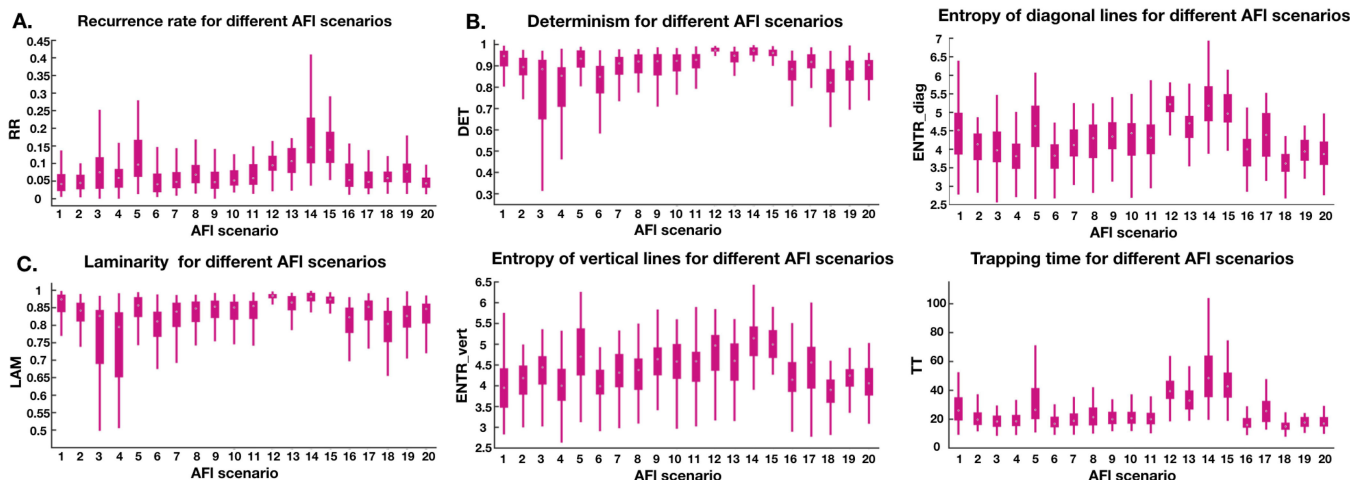
Fig. 5. Effects of the 20 different AFl scenarios on the srRQA features evaluated from the PCS 3. (A). RR attribute. (B). Features related to diagonal lines. (C). Features related to vertical lines.

TABLE III
ROC CURVES FOR THE DISCRIMINATION OF 20 AFL SCENARIOS USING THE SRRQA-BASED FEATURES (MEAN±SD)

	RR	DET	LAM	TT	ENTR_diag	ENTR_vert
AUCROC	0.641±0.002	0.632±0.001	0.628±0.004	0.666±0.002	0.651±0.001	0.626±0.003
Sensitivity	0.325±0.001	0.303±0.001	0.350±0.002	0.215±0.003	0.232±0.001	0.340±0.002
Specificity	0.606±0.001	0.568±0.002	0613±0.001	0.540±0.002	0.542±0.001	0.591±0.001
LOOCV hit rate	0.635±0.078	0.635±0.073	0.625±0.063	**0.654±0.083**	0.650±0.085	0.621±0.058

due to the presence of blocks of recurrence in the calculated RPs Fig. 4.

The icRQA and srRQA-based features extracted from the clinical ECG fit perfectly into the interquartile range of the distribution curves of the parameters extracted from the synthetic data. The similarity between the results obtained from clinical and synthetic data could also be seen from the RPs, as shown in Fig. 6.

IV. DISCUSSION

The 12-lead ECGs are broadly used for cardiac diagnostic and to discriminate AFl from AFib [16]. However, they are rarely applied - if ever - to distinguish among macro-groups of AFl mechanisms - e.g., right-sided AFl vs. left-sided AFl [52].

In the present work, we implemented two RQA frameworks to characterize different AFl mechanisms from the perspective of multivariate surface potentials and nonlinear time series. An inside-out computational simulation generated 12-leads ECGs from 20 AFl mechanisms and different combinations of atrial and torso geometries. This provided an ideal and controlled environment, establishing a consistent ground truth for AFl perpetuation mechanisms without the influence of secondary - or unknown - interfering phenomena, e.g., other simultaneous AFls. Spatio-temporal analysis was achieved by combining PCA and RQA, allowing access to the dynamic structure of the heart activity from the non-invasive perspective.

A specific and representative clinical case of study - a microreentrant AFl in the LA, located at the ant LAA (sc17) - was also analyzed, highlighting the robustness and reliability of the
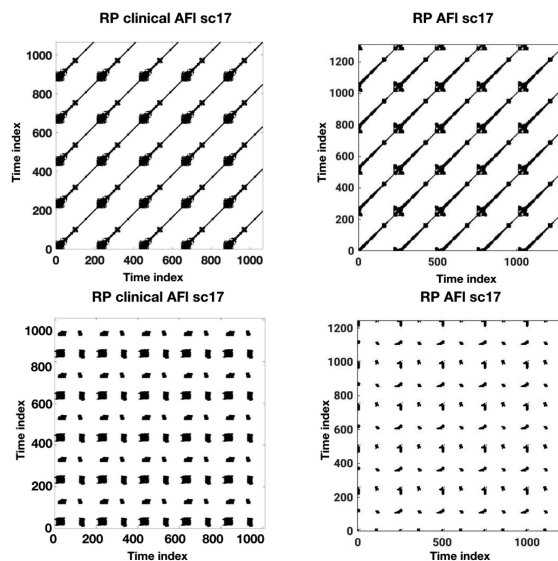
Fig. 6. RPs calculated from the clinical and the corresponding simulated case (left column, and right column, respectively), using icRQA on PCS 1 and srRQA (top line, and bottom line, respectively). The RPs showed how similar the results obtained from the clinical data are in comparison with the simulated ones, using the RQA methods optimized just with synthetic signals. This demonstrates the reliability of the simulated scenarios and the correct implementation of the methods for future clinical application.

proposal. Moreover, having obtained similar results from clinical and synthetic data also demonstrates how these simulated data could really be used in clinical practice. In fact, due to the

limited access to clinical data with a precise description of the ground truth for AFl perpetuation, these simulations could be used as clinical data substitutes to optimize and train RQA and classification algorithms in clinical practice.

Our results suggest that RQA is effective in characterizing and discriminating the dynamic structures from distinct AFl mechanisms, and might help to define novel protocols for clinical planning and ablation strategy.

A. RQA-Based Features Extracted From Simulated AFl 12-Lead ECGs

In the present study, rigorous steps for a proper reconstruction of the RPs and well-defined representative RPs structures (e.g., laminar diagonals, laminar verticals, well-defined blocks etc). Moreover, the introduction of PCA has been shown effective for building a minimal, non-redundant base for the representation of non-invasive multivariate AFl mechanisms. This is corroborated by the variance explained by the selected PCSs and the well-defined RPs structures observed after such coordinate transformation. The need for low dimensional (informative) state space is also justified by the underlying challenges concerning embedding definitions, in which redundant dimensions - as introduced by the spatial oversampling of cardiac activity by multi-lead recording - can contribute to a topological degenerated "attractor". In fact, the addition of non-informative embedding dimensions can introduce spurious RQA structures, as shown by [21], in which a higher dimensional space introduced spurious diagonal lines and inflated the determinism obtained from (uncorrelated) stochastic observations.

It also worth to mention that PCA allows to easily sort PCS according to their information content - explanation of the total variance. In the srRQA case, this allows to implement the state space starting from the two most relevant components - i.e., PCS 1 and PCS 2 -, and then adding new PCS/dimensions following the order of relevance - PCS 3, PCS 4, etc. This would not be possible by using the ECG directly, as there is no natural way to order the leads according to relevance. The 3 main PCSs were taken into account for the icRQA, whereas for the srRQA the embedding dimension used up to the first 5 PCSs. However, the best srRQA embedding dimension was the one using the first 3 PCS (see *Supplementary Materials*), confirming that the following PCS do not contain useful information for the analysis - the main 3 PCSs already explained $99 \pm 0.94\%$ of all variability of the phenomena.

A thorough investigation was then conducted to better define ε for each simulation. The determination of ε took into account the fact that 12-lead ECGs of AFl are usually quite regular - as shown in Fig. 1C - and exhibit high DET as an intrinsic behavior, which would contribute to a high RR and far from the suggested 1% recommendation [21]. The proposed approach aimed to choose an adaptive ε as a percentage of maximal phase space difference, leading to a relatively low RR and distinguishable between the 20 different AFl scenarios in the DET and LAM features.

The minimum diagonal/vertical line length for the calculation of both DET and LAM has also been assessed. The results suggest that DET and LAM are preserved even for different minimum line diagonal/vertical lengths. Undesirable saturation behavior was avoided and AFl discrimination was improved selecting the following minimum diagonal/vertical line lengths for DET and LAM determination: regarding the icRQA, a minimum diagonal length of 13, 16, and 13, and a minimum vertical length of 10, 11, and 18 were selected on PCS1, 2, and 3 respectively; regarding the srRQA, a minimum diagonal length of 6, and a minimum vertical length of 7 were selected.

B. Characterization of Simulated AFl Signals Using RQA

In this work we attempted to (i) assess changes in RQA-based features between different AFl mechanisms; (ii) implement a novel RQA paradigm that also considers spatial information and; (iii) evaluate 12-lead ECG classification using RQA-based features.

The RPs for both methods (icRQA and srRQA) highlighted the highly periodic behaviour of the AFl mechanisms Fig. 2, Fig. 4. These results are corroborated by the ground truth from the simulated AFl episodes, known to be periodic and stable phenomena.

Previous work have shown underlying deterministic structures present on activation sequences on AFib intra-cardiac electrograms [26], [53]. On the one hand, our results from the icRQA paradigm Fig. 2 - also highlights diagonal structures associated with deterministic behavior in the RPs. This may suggest the presence of stable periodic orbits that commonly drive AFl as a localized self-perpetuating loop. However, this deterministic behavior is clearly presented in the RPs obtained in the srRQA paradigm (Fig. 4), which is probably justified by the use of a completely different embedding space defined by the PCS. In this case, the introduction of spatial information seems to contribute to enhancing the laminar behavior - blocks in the RPs - instead of the diagonal lines associated with co-evolution of states. In fact, the AFl scenarios with evident blocks of recurrence are also the ones with the highest values of ENTR_vert, LAM, and TT - sc12, 13, 14, and 15 - for both methods Fig. 2, Fig. 4.

The only scenarios having an iso-line in their 12-lead ECGs are the four focal sources mechanism. These are the only mechanisms in which there is a clear phase of depolarization, repolarization, and rest of the atrial tissue. This might explain the so dominant laminar structure in comparison with all the other mechanisms.

Considering all the features calculated with both RQA methods, the focal source scenarios are the only ones presenting up-regulated RQA-features compared to the other mechanisms. Interestingly, despite representing a scar-related reentry mechanism, sc5 is the only scenario not statistically different from the focal sources episodes considering all srRQA and icRQA features extracted from PCS 1. More specifically, the focal sources on sc12 to sc15 are located nearby the PVs and, since sc5 represents a scar-related reentry within the LPV, the macroscopic behavior of these seemingly different EP are perceived as similar.

Finally, scenarios sc18 and sc20 have shown down-regulated RQA-features, suggesting that microreentries result in lower

deterministic and laminar phenomena in comparison with the other mechanisms.

C. RQA-Based Features Discrimination of Different AFl

Almeida *et al.* showed that RQA-based features are sensitive to EP characteristics of the atrial tissue [28]. Our results support this perspective, suggesting that the RQA-based features extracted from simulated 12-lead ECGs are sensitive to different AFl mechanisms.

Considering that a single feature classification of 20 classes, sometimes very similar between each other, is not trivial, an averaged LOOCV hit rate higher than 60% for all the features with both the methods confirm the hypothesis of using these features as discriminatory features.

Previous works have considered RQA features to classify AFib atrial substrate and use these features as complementary tools to help guide ablation [54]. RQA has also been used to distinguish atrial regions hosting spiral wave reentry from regions with multiple wavelet breakup [55]. Other works combined RQA with PCA on electrograms to discriminate persistent AFib from paroxysmal AFib [27] and non-linear features to discriminate AFib, AFl, VT, and VF [56], [16]. Finally, Yang combined RQA with spatial cardiac vectocardiogram signals to identify cardiovascular disorders [30]. To the best of our knowledge, ours represents the first study to use RQA in the discrimination of different AFl mechanisms from simulated 12-lead ECGs.

The icRQA-based variables Fig. 3 - related to the diagonal lines have shown a higher hit rate on the PCS 3, suggesting that small but important changes in the deterministic behavior of these different types of AFl are present. This can be explained considering that PCS 3 is a signal with a low explanation of the variability, and meaning that it contains only the details of the deterministic behavior of the AFls. By contrast, PCS 1, and 2 have a lower hit rate, likely because there are no major changes regarding the deterministic behavior between the 20 AFl scenarios. Substantially because being PCS 1, and 2 signals with most of the explanation of the variability, they capture the more general deterministic behavior of the mechanisms. The opposite was found for LAM and ENTR_vert, meaning that these AFl mechanisms have shown macro changes on the laminar behavior rather than micro changes.

The findings described here motivate further investigation regarding the use of RQA-based features as biological markers that can potentially be used as features for classification structures to inversely predict the mechanism driving AFl using RQA-features as a basis for a more complex multi-feature classifier with the perspective of guiding ablation procedures in the future.

V. Limitations

The current study is limited to simulated data and tested on only one clinical ECG.

Although 20 AFl mechanisms inspired by clinical situations have been implemented, they are just a general representation of the mechanisms that are most commonly found in the literature. More scenarios should be included in the dataset, considering the heterogeneity found in the clinical practice - e.g., different locations of scar-related AFl or slow conduction areas.

Further investigations should be conducted on more clinical data to extend the value of the methods. Although the manual segmentation of the clinical ECG is not time consuming, in view of a future clinical application, automated segmentation of clinical ECG should be implemented to extract the F-wave.

The embedding for the estimation of RPs and, consequently, RQA parameters has been done considering the ability of the variables in discriminating the different types of AFl scenarios. The fact that 20 different classes have been used could have led to a biased parameters setting. Accordingly, while it could have increased the differences between some classes, it might have decreased the differences between others, leading to a non-optimal discrimination among them. Therefore, a reduction of the number of classes - e.g., by merging some cases in the same class - should be investigated. The merging could also lead to an increase in the hit rates, making the classification problem easier. The grouping could be done by gathering classes belonging to the same macro-areas - e.g. macroreentry, microreentry, scar-related reentry, figure-8, and focal sources - or in AFl classes that requires similar ablation procedures to be terminated.

The AFl mechanisms were simulated with atrial models without ventricles. Thus, the QRS-T complex was absent from our signals. This must be taken into account when applying the RQA methods to clinical data. In addition, the CV set in the simulations is constant and only 8 atria models were used. A change in the CV and the addition of other atria models could lead to a change in the results.

A single feature classification was performed to evaluate the potential of these variables to discriminate different AFl mechanisms. To implement a valid classifier able to inversely predict the AFl mechanism from the ECG signals and increase the hit rate with both the methods, a multi feature classification and different classification algorithms should be tested.

Despite of that, this work presents an important contribution for characterizing the dynamics of AFl mechanisms, which deserves a careful attention for setting the RQA general approach and parameters before class clustering and classification evaluation.

VI. Conclusion

In the present work, different AFl mechanisms were characterized from the perspective of multivariate surface potentials and nonlinear time series. Two methods for RQA were implemented to investigate different AFl scenarios. An inside-out computational simulation generated 12-leads ECGs from 20 AFl mechanisms and different combinations of atrial and torso geometries, in which the ground truth for AFl perpetuation were known. RQA was combined with PCA creating a spatial-temporal domain analysis, allowing access to the dynamic structure of the heart activity from the non-invasive perspective.

Our results suggest that RQA-based features are sensitive to the underlying EP phenomena, and are effective in characterizing the dynamic structures from distinct AFl mechanisms.

The focal source scenarios showed the highest RQA feature values using both paradigms, demonstrating how these cases have a significant deterministic and laminar behavior in the dynamic structure. In contrast, microreentries are less deterministic and laminar phenomena.

The use of the PCSs 1, 2, and 3 for the icRQA showed how there can be relevant small or major changes in the dynamic behaviors between these different AFl mechanisms, based on the ability to better or worse discriminate the AFl along the three PCSs.

RQA-based features could potentially be used to implement a multi-feature classifier able to inversely predict different mechanisms driving AFl from non-invasive signals in future works. This non-invasive RQA-based classifier could aid in planning and tailoring the ablation strategy, reducing time and resources required to conduct invasive cardiac mapping and ablation procedures.

To conclude, a clinical 12-lead ECG was used as a proof of concept to show the efficacy on using simulations in that cases in which to obtain reliable clinical data would be difficult, and to prove the validity of these two RQA methods to characterize and to classify these different AFl mechanisms.

ACKNOWLEDGMENT

REFERENCES

[1] J. Granada *et al.*, "Incidence and predictors of atrial flutter in the general population," *J. Amer. College Cardiol.*, vol. 36, no. 7, pp. 2242–2246, 2000.

[2] S. Bun *et al.*, "Atrial flutter: More than just one of a kind," *Eur. Heart. J.*, vol. 36, no. 35, pp. 2356–2363, 2015.

[3] F. G. Cosio *et al.*, "Atrial flutter: An Update," *Rev. Esp. Cardiol.*, vol. 59, no. 8, pp. 816–831, 2006.

[4] F. G. Cosio *et al.*, "Atrial flutter mapping and ablation I: Studying atrial flutter mechanisms by mapping and entrainment," *Pacing Clin. Electrophysiol*, vol. 19, no. 5, pp. 841–853, 1996.

[5] R. J. Schilling *et al.*, "Characterization of the anatomy and conduction velocities of the human right atrial flutter circuit determined by non-contact mapping," *J. Am. Coll. Cardiol.*, vol. 38, no. 2, pp. 385–393, 2001.

[6] T. Itoh *et al.*, "High correlation of estimated local conduction velocity with natural logarithm of bipolar electrogram amplitude in the reentry circuit of atrial flutter," *J. Cardiovascular Electrophysiol.*, vol. 25, no. 4, pp. 387–394, 2014.

[7] G. Ndrepepa *et al.*, "Activation patterns in the left atrium during counterclockwise and clockwise atrial flutter," *J. Cardiovascular Electrophysiol.*, vol. 12, no. 8, pp. 893–899, 2001.

[8] P. Jais *et al.*, "Mapping and ablation of left atrial flutters," *Circulation*, vol. 101, no. 25, pp. 2928–2934, 2000.

[9] I. Deisenhofer *et al.*, "Left atrial tachycardia after circumferential pulmonary vein ablation for atrial fibrillation: Incidence, electrophysiological characteristics, and results of radiofrequency ablation," *Europace*, vol. 8, no. 8, pp. 573–582, 2006.

[10] S. Ammar *et al.*, "Ablation of perimitral flutter: Acute and long-term success of the modified anterior line," *Europace*, vol. 17, no. 3, pp. 447–452, 2015.

[11] A. M. Patel *et al.*, "Atrial tachycardia after ablation of persistent atrial fibrillation: Identification of the critical isthmus with a combination of multielectrode activation mapping and targeted entrainment mapping," *Circ. Arrhythmia Electrophysiol.*, vol. 1, no. 1, pp. 14–22, 2008.

[12] S. M. Markowitz *et al.*, "Atrial tachycardias and atypical atrial flutters: mechanisms and approaches to ablation," *Arrhythmia Electrophysiol. Rev.*, vol. 8, no. 2, pp. 131–137, 2019.

[13] R. De Ponti *et al.*, "Treatment of macro-re-entrant atrial tachycardia based on electroanatomic mapping: Identification and ablation of the mid-diastolic isthmus," *Europace*, vol. 9, no. 7, pp. 449–457, 2007.

[14] P. Jais *et al.*, "A deductive mapping strategy for atrial tachycardia following atrial fibrillation ablation: Importance of localized reentry," *J. Cardiovascular Electrophysiol.*, vol. 20, no. 5, pp. 480–491, 2009.

[15] C. Pedrinazzi *et al.*, "Atrial flutter: From ECG to electroanatomical 3D mapping," *Heart Int.*, vol. 2, no. 3-4, pp. 161–170, 2006.

[16] U. R. Acharya *et al.*, "Automated characterization of arrhythmias using nonlinear features from tachycardia ECG beats," in *Proc. IEEE Int. Conf. Syst., Man, Cybern.*, Budapest, 2016, pp. 533–538.

[17] L. L. Trulla *et al.*, "Recurrence quantification analysis of the logistic equation with transients," *Phys. Lett. A*, vol. 223, no. 4, pp. 255–260, 1996.

[18] C. L. Webber Jr. and J. P. Zbilut, "Dynamical assessment of physiological systems and states using recurrence plot strategies," *J. Appl. Physiol.*, vol. 76, no. 2, pp. 965–973, 1994.

[19] J. P. Zbilut *et al.*, "Recurrence quantification analysis as a tool for nonlinear exploration of nonstationary cardiac signals," *Med. Eng. Phys.*, vol. 24, no. 1, pp. 53–60, 2002.

[20] N. Marwan *et al.*, "Recurrence-plot-based measures of complexity and their application to heart-rate-variability data," *Phys. Rev. E.*, vol. 66, no. 2, 2002, Art. no. 026702.

[21] N. Marwan *et al.*, "Recurrence plots for the analysis of complex systems," *Phys. Rep.*, vol. 438, pp. 237–329, 2007.

[22] H. Arce *et al.*, "Recurrence analysis of cardiac restitution in human ventricle," in *Recurrence Plots and Their Quantifications: Expanding Horizons*, Springer Proceedings in Physics, vol. 180. Berlin, Germany: Springer, 2016, pp. 169–183.

[23] U. R. Acharya *et al.*, "Automated prediction of sudden cardiac death risk using Kolmogorov complexity and recurrence quantification analysis features extracted from HRV signals," in *Proc. IEEE Int. Conf. Syst., Man, Cybern.*, 2015, pp. 1110–1115.

[24] M. Tang *et al.*, "An improved method for discriminating ECG signals using typical nonlinear dynamic parameters and recurrence quantification analysis in cardiac disease therapy," in *Proc. IEEE Eng. Med. Biol.*, 2005, pp. 2459–2462.

[25] U. Desai *et al.*, "Diagnosis of multiclass tachycardia beats using recurrence quantification analysis and ensemble classifiers," *J. Mech. Med. Biol.*, vol. 16, no. 1, 2016, Art. no. 1640005.

[26] F. Censi *et al.*, "Recurrent patterns of atrial depolarization during atrial fibrillation assessed by recurrence plot quantification," *Ann. Biomed. Eng.*, vol. 28, pp. 61–70, 2000.

[27] S. Zeemering *et al.*, "Recurrence quantification analysis applied to spatiotemporal pattern analysis in high-density mapping of human atrial fibrillation," in *Proc. IEEE Eng. Med. Biol.*, 2015, pp. 7704–7707.

[28] T. Almeida *et al.*, "Characterization of human persistent atrial fibrillation electrograms using recurrence quantification analysis," *Chaos*, vol. 28, no. 8, 2018, Art. no. 085710.

[29] T. Almeida *et al.*, "The temporal stability of recurrence quantification analysis attributes from chronic atrial fibrillation electrograms," *Res. Biomed. Eng.*, vol. 34, no. 4, pp. 337–349, 2018.

[30] H. Yang, "Multiscale recurrence quantification analysis of spatial cardiac vectorcardiogram signals," *IEEE Trans. Biomed. Eng.*, vol. 58, no. 2, pp. 339–347, Feb. 2011.

[31] P. Jais *et al.*, "A deductive mapping strategy for atrial tachycardia following atrial fibrillation ablation: Importance of localized reentry," *J. Cardiovascular Electrophysiol.*, vol. 20, no. 5, pp. 480–491, 2009.

[32] J. E. Ban *et al.*, "Relationship between complex fractionated atrial electrograms during atrial fibrillation and the critical site of atrial tachycardia that develops after catheter ablation for atrial fibrillation," *J. Cardiovasc. Electrophysiol.*, vol. 25, no. 2, pp. 146–153, 2014.

[33] T. G. Oesterlein *et al.*, "Automatic identification of reentry mechanisms and critical sites during atrial tachycardia by analyzing areas of activity," *IEEE Trans. Biomed. Eng.*, vol. 65, no. 10, pp. 2334–2344, Oct. 2018.

[34] V. Jacquemet, "An eikonal approach for the initiation of reentrant cardiac propagation in reaction-diffusion models," *IEEE Trans. Biomed. Eng.*, vol. 57, no. 9, pp. 2090–2098, Sep. 2010.

[35] J. Trächtler *et al.*, "Virtualizing clinical cases of atrial flutter in a fast marching simulation including conduction velocity and ablation scars," *Current Directions Biomed. Eng.*, vol. 1, no. 1, pp. 405–408, 2015.

[36] M. W. Krueger *et al.*, "Personalization of atrial anatomy and electrophysiology as a basis for clinical modeling of radio-frequency ablation of atrial fibrillation," *IEEE Trans. Med. Imag.*, vol. 32, no. 1, pp. 73–84, Jan. 2013.

[37] A. Wachter *et al.*, "Mesh structure-independent modeling of patient-specific atrial fiber orientation," *Current Directions Biomed. Eng.*, vol. 1, no. 1, pp. 409–412, 2015.

[38] A. Loewe *et al.*, "Influence of the earliest right atrial activation site and its proximity to interatrial connections on P-wave morphology," *Europace*, vol. 18, no. suppl 4, pp. iv35–iv43, 2016.

[39] A. Loewe, "Chronic AF induced remodeling," in *Modeling Human Atrial Patho-Electrophysiology From Ion Channels to ECG : Substrates, Pharmacology, Vulnerability, and P-Waves*, Karlsruhe, Germany: KIT Scientific Publishing, 2016, ch. 5.2, pp. 113–119.

[40] R.L. Lux *et al.*, "Body surface potential mapping techniques," in *Comprehensive Electrocardiology*. London, U.K.: Springer, 2010, pp. 1361–1374.

[41] M. Stenroos, "The transfer matrix for epicardial potential in a piece-wise homogeneous thorax model: The boundary element formulation," *Phys. Med. Biol.*, vol. 54, no. 18, pp. 5443–55, 2009.

[42] R. Schmidt *et al.*, "Herzerregung: Elektrokardiogramm (EKG)," in *Physiologie Des Menschen: Mit Pathophysiologie*, Berlin, Germany: Springer-Verlag, 2011, ch. 25.3, pp. 578–588.

[43] A. Izenman, "Linear dimensionality reduction," in *Modern Multivariate Statistical Techniques: Regression, Classification, and Manifold Learning*, New York, NY, USA: Springer, 2008, ch. 7.2, pp. 196–215.

[44] A. Khawaja, "Automatic ECG analysis using principal component analysis and wavelet transformation," Ph.D. dissertation, Dept. Elect. Info. Eng., Karlsruhe Inst. Technol., Karlsruhe, Germany, 2007.

[45] J. Shlens, "A tutorial on principal component analysis," 2014, *arXiv:1404.1100*.

[46] J.-P. ECKmann *et al.*, "Recurrence plots of dynamical systems," *Europhys. Lett.*, vol. 4, no. 9, pp. 973–977, 1987.

[47] P. Faure and H. Korn, "A new method to estimate the Kolmogorov entropy from recurrence plots: its application to neural signals," *Physica D: Nonlinear Phenom.*, vol. 122, pp. 265–279, 1998.

[48] N. Marwan, "How to avoid potential pitfalls in recurrence plot based data analysis," *Int. J. Bifurcation Chaos*, vol. 21, pp. 1003–1017, 2011.

[49] J. P. Zbilut and C. L. Webber Jr., "Embeddings and delays as derived from quantification of recurrence plots," *Phys. Lett.*, vol. 171, no. 3-4, pp. 199–203, 1992.

[50] M. Hollander *et al.*, *Nonparametric Statistical Methods*, 3rd ed., Hoboken, NJ, USA: Wiley, 2013, ch. 5-6.

[51] J. D. Gibbons and S. Chakraborti, "Tests of the equality of k indipendent samples," in *Nonparametric Statistical Inference*, 5th ed. Boca Raton, FL, USA: CRC Press, 2011, ch. 10, pp. 343–377.

[52] C. Medi and J. M. Kalman, "Prediction of the atrial flutter circuit location from the surface electrocardiogram," *Europace*, vol. 10, pp. 786–796, 2008.

[53] D. Gordon *et al.*, "Searching for "order" in atrial fibrillation using electrogram morphology recurrence plots," *Comput. Biol. Med.*, vol. 65, pp. 220–228, 2015.

[54] N. Navoret *et al.*, "Detection of complex fractionated atrial electrograms using recurrence quantification analysis," *IEEE Trans. Biomed. Eng.*, vol. 60, pp. 1975–1982, 2013.

[55] J. P. Hummel *et al.*, "A method for quantifying recurrent patterns of local wavefront direction during atrial fibrillation," *Comput. Biol. Med.*, vol. 89, pp. 497–504, 2017.

[56] D. DeMazumder *et al.*, "Dynamic analysis of cardiac rhythms for discriminating atrial fibrillation from lethal ventricular arrhythmias," *Circ. Arrhythmia Electrophysiol.*, vol. 6, no. 3, pp. 555–561, 2013.